Continuous fractionation of nanoparticles based on their magnetic properties applying simulated moving bed chromatography

Carsten-Rene Arlt, Dominik Brekel, Matthias Franzreb *

Institute of Functional Interfaces, Karlsruhe Institute of Technology, Hermann-von-Helmholtz-Platz 1, 76344 Eggenstein-Leopoldshafen, Germany

A B S T R A C T

The production of high-quality and pure nanoparticles is becoming increasingly important from an industrial perspective. Current and emerging applications of high-quality nanoparticles include among others medical uses, analytical products or functional pigments. Often the initial synthesis does not deliver the required quality with respect to uniform size and composition, resulting in the need of additional purification and fractionation steps. However, technical fractionation of nanoparticles is still a challenge, especially if looking for continuous processes. If the impurities are within a similar size range than the target particles, classical processes, such as filtration, are often not suitable. In this study a novel and easily scalable system is presented, which can continuously fractionate nanoparticles by their magnetic properties. The system is based on the principle of magnetic chromatography, which allows to control the interaction between nanoparticles and a magnetizable stationary phase by means of an external magnetic field. Running a single chromatography column in pulse mode for the fractionation of diamagnetic and superparamagnetic nanoparticles, peak resolutions of the separated particle fractions of 0.93 could be achieved. Continuous operation could be realized by transferring the principle into a simulated moving bed system including four columns. This allowed continuous feed streams of nanoparticles with a space time yield of 27.5 mg/(L·min) to be fractionated. Recovery rates of up to 98% were achieved, while the contaminant depletion up to 100% could be accomplished. Based on these results we see our process as a potential alternative to demanding and expensive nanoparticle fractionation methods, such as ultracentrifuges, requiring less energy and including no quickly rotating parts.

1. Introduction

The use of nanoparticles, which are particles in the size range below 1000 nm, is becoming increasingly important from a technical perspective. They offer many advantages like the enhancement of mass as well as electron transfer effects [1–3] and they are available in a wide chemical and morphological diversity [4]. This enables fields of application such as data storage [5], vaccines [6], biosensors [7], polymeric nanoparticle based materials [8], magnetic hyperthermia [9,10] and targeted drug therapy [11–13]. However, the purification of heterogeneous nanoparticle mixtures is still problematic. Properties such as the colloidal aggregation behavior [14] and a large surface-to-volume ratio complicate the purification process [15]. Therefore potential undesirable impurities that have been generated in the production process, such as residual polymers, abrasion and by-products etc., must be removed. While smaller impurities such as solvents or monomers can be removed by dialysis [16] or membrane filtration [17], only few processes exist for the classification of target nanoparticles and impurities if they are of the same size [18,19].

For this reason, other novel approaches for nanoparticle fractionation have been investigated. For example, acoustic methods have been demonstrated for lab-on-a-chip processes [20]. Furthermore, charge differences of the nanoparticles could be used for gel electrophoresis by coating a capillary with a charged polymer layer [21], or selective electrophoretic deposition [22]. Another interesting approach is the use of liquid chromatographic methods for the effective fractionation of nanoparticles. In such a process, nanoparticle suspensions in buffers, which represent the mobile phase, are separated by differences in their interactions with a separation matrix, the so-called stationary phase. Size exclusion chromatography (SEC) for nanoparticle classification in lab scale has already been successfully demonstrated [23]. However, in SEC the separation limits are defined by the pore sizes of the available separation matrix. Furthermore, the investigation is limited to particles of different sizes. For this reason, a different separation mechanism will be pursued in this work. In order to separate nanoparticles of similar size, shape and density, the magnetic susceptibility of different materials is used as a separating attribute. The magnetic volume susceptibility χ_m is a material characteristic describing the relationship between the particle magnetization M_p and the external magnetic field strength H:

$$\chi_m \quad \frac{M_p}{H} \tag{1}$$

The magnetic susceptibility is a constant for dia- and paramagnetic substances, whereas for ferri- and ferromagnetic substances it is, inter

* Corresponding author.
E-mail address: matthias.franzreb@kit.edu (M. Franzreb).

Nomenclature

ε_t	Column porosity
t_0	Column void time
V_c	Column volume
m_i	Dimensionless flow rate ratio
Q_i	Flow rate
H_i	Henry coefficient
H	Magnetic field strength
F_m	Magnetic force
V_P	Particle volume
M_p	Particle magnetization
w_{hi}	Peak width at medium peak height
t_{Ri}	Retention time
R	Resolution
χ_m	Susceptibility
t_s	Switching time
μ_0	Vacuum permeability constant

alia, a function of particle shape and size as well as of the field strength. As in general the material of the nanoparticles of interest is defined, the susceptible variables regarding the attainable magnetic force are the prevailing field strength and especially its gradient. The resulting magnetic force F_m can be described as:

$$F_m \quad \mu_0 V_p M_p \nabla H \tag{2}$$

In which μ_0 is the vacuum permeability constant and V_P the particle volume. In the case of ferri- or ferromagnetic particles larger than approx. 2 μm, the forces relevant for particle behavior in suspensions are primarily the magnetic force and the hydrodynamic resistance force. In case of smaller particles, in addition the influence of Brownian molecular motion on the particle behavior must be taken into account. Instead of clearly defined particle paths, the statistical nature of Brownian motion enforces the concept of treating ferri- or ferromagnetic nanoparticles as an ensemble having a continuous concentration distribution. The tendency of the nanoparticles to concentrate within the regions of highest magnetic field is opposed by diffusion, which tries to level out concentration gradients.

A simple setup for magnetic chromatography has been introduced by Nomizu et al. [24]. They filled a small column with magnetizable stainless steel beads and surrounded the column with an electromagnetic coil. Applying an intermittent magnetic field, they could show the retention of an injected pulse of a magnetite suspension, but the relatively coarse steel bead matrix which was vibrated resulted in a low peak quality. In a previous work of ours, some drawbacks of the setup of Nomizu et al. could already be solved [25]. By the use of a more efficient operation mode applying a constant magnetic field of reduced strength and a finer stationary matrix, a successful size fractionation of magnetically active nanoparticles could be achieved. In the work described here, the magnetic susceptibility is introduced as an additional parameter in the fractionation of ultrafine particles by using magnetic chromatography. A well-established process for the separation of micro and nanoparticles according to their magnetic properties is found in High Gradient Magnetic Separation (HGMS) [26–28]. In hitherto existing HGMS processes, however, only a discontinuous mode of operation is used and the process usually cannot distinguish between particle types, which show only moderate differences in their magnetic susceptibilities. This leads to unwanted system downtimes and to a higher consumption of mobile phases. Also in the case of particle fractionation by their magnetic susceptibility there exists a pioneering paper of Nomizu et al. [29]. They applied an open tubular column in combination with strong magnetic fields to separate pulses of nanoparticles on the basis of their susceptibility. Therefore, also the magnetic chromatography process suggested by Nomizu is a batch processes. In contrast, the approach described here has the goal to transfer cyclic magnetic chromatography into a continuous and scalable process by the application of the so-called Simulated Moving Bed (SMB) principle. With its origins in the petrochemical industry, SMB has become increasingly important as a separation method of dissolved molecules, particularly in the pharmaceutical sector [30]. SMB enables the separation of e.g. enantiomers [31,32] or macromolecules [33], but has not been applied for nanoparticle fractionation so far. The only exception can be found in a work of Jungbauer et al. [34] who used SMB to separate protein aggregates from the original buffer in which they were suspended. However, also in this case the aim was not the fractionation of different nanoparticle species. Using magnetic chromatography, this work aims to develop an SMB system capable to fractionate nanoparticles of uniform size according to their susceptibility. In the beginning, single column experiments were conducted to determine the process parameters required to design the SMB process. Subsequently, the SMB setup was assembled and different operation modes for successful nanoparticle fractionation were evaluated by analyzing the separation quality.

2. Experimental

2.1. Chemicals and reagents

In this study two nanoparticle combinations were evaluated. Both combinations consist of silica nanoparticles and a second nanoparticle type of which a fraction of the particle mass consisted of a magnetic iron oxide (maghemite or magnetite). While the silica particles show only a very weak repulsive interaction with a magnetic field [35], the nanoparticles containing iron oxides show superparamagnetic behavior. The first particle mixture, which was mainly used for preliminary studies, is a combination of silica particles (sicastar 100 nm, micromod Partikeltechnologie GmbH, Rostock, Germany) and cluster-like dextran-iron oxide composite particles (nanomag-D-spio 100 nm, micromod Partikeltechnologie GmbH, Rostock, Germany). Both nanoparticle types were commercially sourced and, according to the manufacturer, had a nominal size of 100 nm. Besides the identical size, the densities of the two nanoparticle types are rather close, 2 g/cm^3 for silica particles and 1.4 g/cm^3 for the cluster-like particles. The cluster-like particles show a saturation magnetization of about 6.1 Am^2/kg. The second combination of particles consisted of silica nanoparticles (sicastar 50 nm, micromod Partikeltechnologie GmbH, Rostock, Germany) and superparamagnetic core–shell particles with a maghemite core, surrounded by a dextran shell (synomag 50 nm, micromod Partikeltechnologie GmbH, Rostock, Germany). Again, both nanoparticle types were commercially sourced and, according to the manufacturer, had a nominal size of 50 nm. The core–shell particles have a saturation magnetization of 48 Am^2/kg and a density of 2.5 g/cm^3. Due to the improved magnetic properties, this second particle mixture was used for further investigations in the continuous processes.

The borosilicate glass chromatography columns (Diba Industries Inc., Danbury, Connecticut) used in this work had an inner diameter of 6.6 mm and formed a chromatography bed length of 120 mm. A PTFE frit each at the beginning and end of the glass column with a pore size of 5 μm served as a filter to retain the matrix material and exclude larger impurities. As stationary phase within the magnetic chromatography columns a stainless-steel powder Truform 174 (Praxair Surface Technologies, Ratingen, Germany) fabricated for 3D selective laser melting (SLM) was used. The particles consist of a chromium rich (12.5%) alloy with small amounts of carbon, silicon and manganese. Their particle size distribution ranges from 5 to 50 μm with a D_{50} value of 31 μm. The particles show a high saturation magnetization of 150 Am^2/kg, a very small remanence of 95 mAm^2/kg and a coercivity of 160 A/m. Due to its low remanence, this column material showed no relevant residual magnetization even after several magnetizations, making it suitable for continuous use.

2.2. Experimental setup

The used magnetic field source consists of a Helmholtz coil arrangement including four coils (average diameter: 7.58 cm) placed in the distance of the coil radius to generate a nearly homogeneous field in the center of the arrangement. With this set-up, a magnetic field strength increasing linearly with the applied current could be generated. At a current of 2.4 A a magnetic field strength of 17 mT was achieved. The necessary current was supplied by a laboratory power supply unit (Distrelec Group AG, Uster, Switzerland), which could supply voltages of up to 30 V and currents of up to 5 A. Further details of the used magnetic field source can be found in the Supporting Information. The chromatographic columns used for this work are described in 2.1. Depending on the operation mode applied, one or several of these columns were installed in a suitable chromatographic system. For single column experiments, an FPLC (Fast Protein Liquid Chromatography) system (Akta purifier, GE Healthcare, Buckinghamshire, England) equipped with PEEK tubings with an inner diameter of 0.25 mm was used. In the course of an experiment, the injected sample was pumped through the column at a constant flow rate of 4 mL/min. The effluent of the column was constantly analyzed by two flow through measuring cells, registering UV intensity at 280 nm and conductivity. If the effluent had to be collected for further analysis, a fraction collector dividing the effluent into samples of 0.25 mL volume could be used. The amount of sample injected was 100–500 µL in each experiment. In order to guarantee a stable dispersion of the nanoparticle mixture, a buffer system had to be found in which no nanoparticle type tends to agglomerate. A dilute Tris buffer (1 mM) having a pH value of 9.5 fulfilled this condition and was used as mobile phase being pumped through the column in all experiments. After each experimental run, the column was flushed with buffer without the application of a magnetic field in order to remove any residual material.

The experiments for the continuous fractionation of the nanoparticle mixtures were carried out in an AZURA Lab Simulated Moving Bed (SMB) System (Knauer Wissenschaftliche Gerate GmbH, Berlin, Germany). A SMB approximates a continuous counter-current operation mode of a chromatographic system, in which the stationary phase moves in opposite direction to the flow direction of the mobile phase. The approximation is achieved by the use of multiple separation zones and a cyclic interchange of the positions of feed and eluent inlet as well as raffinate and extract outlet by switching valves. In the configuration used in this work, four separation zones were used. If the flow rates of the mentioned in- and outflows as well as the cycle time for switching are chosen correctly, a SMB can achieve a continuous separation of the species in the feed flow into two effluent fractions. In the course of the separation, the species showing stronger interactions with the stationary phase will end up in the extract and the species showing weaker interaction with the stationary phase will end up in the raffinate. PEEK tubings with an inner diameter of 0.75 mm were used for the connection of the columns and the valves. The flow is controlled by three piston pumps within the loop system and a feed pump. The flow direction is controlled by seven multi-position valves and by eight check valves. This arrangement would allow the integration of up to eight columns in the system, however, all SMB experiments were conducted by the use of only four columns, one for each zone shown in Fig. 1. By the help of the four pumps, the flow within each zone could be adjusted independently. The online analysis of the extract and the raffinate was performed using two UV cells at 280 nm. Because of the periodically fluctuating effluent concentrations extract and raffinate samples were pooled over several complete switching cycles for further analyses. For an alternative way of operation, the system also includes a manual valve that can open the circuit after zone 4 and before the eluent inflow. In order to exclude a loss of pump performance due to possible damage by nanoparticles, the flow rate of the pumps was checked before each experiment.

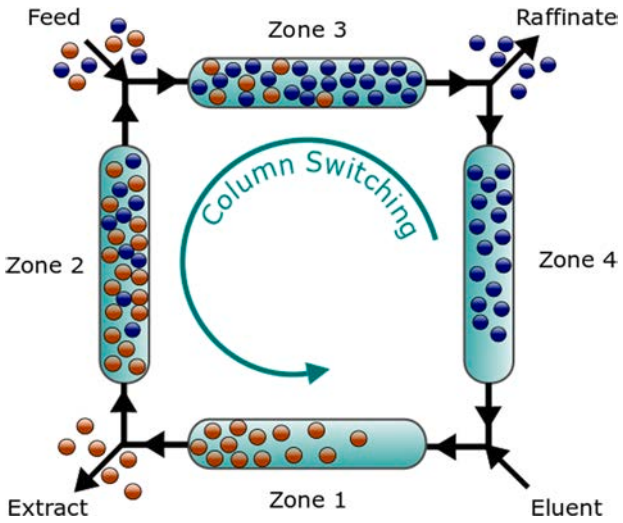

Fig. 1. Scheme of a Simulated Moving Bed process with a four-column configuration.

2.3. Experimental procedure

All columns were packed applying the procedure described in the following. Since the material showed fast settling rates due to its high density, discrete amounts of slurry were pipetted into the column during a fast pump pulse lowering the protruding fluid level to avoid sedimentation-related layering. The separation matrix was finalized under a flow of 10 mL/min for 15 min. The quality of the separation column packing was controlled by injecting a tracer peak of 1% (v/v) aqueous acetone solution and measuring its asymmetry by means of the resulting UV signal. The quality of the column packing was defined to be acceptable within an asymmetry range of 1–1.4. If the asymmetry was outside of this range, the column was repacked. In the process of a particle retention experiment, first the separation column was equilibrated at a flow rate of 4 mL/min with 10 mL — 3 column volumes— of Tris buffer at a magnetic field of 0 mT. Afterwards the required magnetic field was adjusted by the current of the power source. A pulse of 100 - 500 µL of the nanoparticle suspension was injected at the same flow rate and the pumping of the mobile phase was continued until the UV-Signal in the effluent reached its base line level again. The nanoparticle suspension contained of a mixture of 1.25 g/L silica and 15 mg/L synomag nanoparticles, or a mixture of 1.25 g/L silica and 0.25 g/L iron oxide nanoparticles respectively. This concentration difference was chosen because the synomag particles show an intensive UV absorption and therefore peaks of comparable size are produced. Shortly before use, the required nanoparticle mixture was generated from the respective stock solutions by dilution with the mobile phase (Tris buffer) and retitration to a pH of 9.5. In case of single-column experiments with magnetic field application, the magnetic field was switched off after 5 mL in order to regenerate the column by removing any magnetically bound particles.

For the SMB-experiments all flow rates were adjusted according to the interaction affinities between the nanoparticles and the stationary phase determined in the single column experiments. From the retention factors determined in these experiments, apparent Henry coefficients of the two nanoparticle types can be calculated. These coefficients are then used to calculate the required flow rates by the help of a software tool being part of the SMB control system [36–38]. A list of the resulting flow rates of the individual zones can be found in Tables 1 and 2. The feed solution was continuously fed into the SMB cycle by a feed pump. For each experimental run, the system was equilibrated with pure buffer in the feed and eluent inlet for four cycles in order to fully settle stationary conditions and flush the periphery. After switching the feed to the nanoparticle mixture, the system needed four to eight cycles to reach a

stable quasi-stationary state.

2.4. Analytical methods

The offline analysis of the collected nanoparticle samples was carried out by emission spectrometry with inductively coupled plasma (ICP-OES). The instrument used was an Optima™ 8000 ICP-OES (PerkinElmer Inc., Waltham, MA, USA). In this method, samples to be analyzed are thermally decomposed and ionized in an argon plasma flame. The plasma stimulates the ions to emit light, which enables a quantitative analysis Since the particles used consisted mainly of SiO_2 and $Fe^{2+}(Fe^{3+})_2O_4$. The element analysis was therefore carried out for Si and Fe specific wavelengths.

The determination of the magnetic flux density generated by the electric coils was carried out using a Hall probe (FH 31/4, MAGNET-PHYSIK Dr. Steingroever GmbH, Cologne, Germany). In order to measure the magnetic flux density of the electric coils the Hall probe was repeatedly moved along the cylindrical axis of the coil while varying the applied current.

2.5. Estimation of optimal SMB operation parameters

In order to function properly, SMB chromatography requires carefully selected flow rates in the individual zones. These flow rates are determined from single column experiments. Since simulated moving bed chromatography in the classical sense is a method for a binary separation, a first characteristic for the chances for success of a separation is the resolution R, which is calculated as follows:

$$R \quad 1,18*\frac{(t_{R2} \quad t_{R1})}{(w_{h1} + w_{h2})} \tag{3}$$

Here $t_{R2} \quad t_{R1}$ is the difference of the retention times and $w_{h1} + w_{h2}$ is the sum of the peak widths at medium peak height. At a resolution of 1.5 or above a baseline separation is achieved, at a value of 1 there is an overlap of 3% of the peak area. Therefore, a high resolution determined in a single column experiment, is a good indication that also a continuous separation in a multi-column process should work with high efficiency.

For the SMB process a coordinated selection of the individual flow rates in the four zones illustrated in Fig. 1 is necessary. This proportion can be defined in a dimensionless flow rate ratio m_i as follows [37]:

$$m_i \quad \frac{Q_i * t_s \quad V_c * \varepsilon_t}{V_c * (1 \quad \varepsilon_t)} \tag{4}$$

Here Q_i is the flow rate in the respective zone, V_c is the column volume, t_s is the switching time and ε_t is the column porosity. An essential factor for the design of an SMB process are the so-called Henry coefficients H_i of the substances to be separated. These coefficients can be determined from the retention times of the single-column tests of the individual components:

$$H_i \quad \left(\frac{t_R}{t_0} \quad 1\right) * \frac{\varepsilon_t}{1 \quad \varepsilon_t} \tag{5}$$

Based on the Henry coefficients and the flow rate ratios, the process can now be designed to achieve a stable SMB process with the following conditions according to Mazotti and Morbidelli et al. [36–38]:

$$H_2 \leq m_2 \leq H_1; \quad H_2 \leq m_3 \leq H_1; \quad m_4 \leq H_2; \quad m_1 \geq H_1 \tag{6}$$

3. Results and discussion

3.1. Nanoparticle fractionation without an external magnetic field

In order to investigate the intrinsic magnetic interaction between the nanoparticles and the matrix, an experimental series without external magnetic field was carried out first. The intrinsic magnetic interaction results from the spontaneous magnetization of the synomag nanoparticles. Because of their small size these nanoparticles mainly form single-domain systems, meaning there exists only one orientation of the crystal lattice throughout the particle [39]. This could be explained by the fact that magnetite nanoparticles in this size range are too large to be superparamagnetic but form single domain crystallites in which the atomic magnetic moments are aligned resulting in a spontaneous magnetization of the nanoparticles [40]. On the macroscopic level, the spatial directions of the nanoparticle orientation and the corresponding magnetization are statistically distributed, leading to a mutual extinction. However, looking at the interactions of single nanoparticles with magnetizable macroscopic bodies, the spontaneous magnetization results in an attractive force. The hypothesis was that this attractive force will manifest itself in the form a retention of the nanoparticles even without the application of an external magnetic field. It is worth noting, that this mode of retention, would allow an energy-efficient separation of nanoparticles with comparable physical properties.

In preliminary tests with a single type of nanoparticles it could be proven that injected pulses of silica nanoparticles show a retention time that is slightly higher than that of the unobstructed tracer molecule (see Fig. S2 of the SI). This effect occurred regardless of whether an external magnetic field of up to 14.2 mT was applied or not. In contrast, the synomag and the nanomag nanoparticles show an increased residence time in the column, indicating attractive interactions with the matrix material. However, as shown in a previous work [25], the magnetic nanoparticle peak shows no retention if the magnetizable steel bead matrix is replaced by a matrix consisting of polymethylmethacrylate (PMMA) beads of approx. the same size. This excludes the possibility that the observed retention may be caused by other effects than magnetic interaction, such as e.g. sieving effects. In the following fractionation experiments injecting a mixture of silicate and synomag particles a flow rate of 4 mL/min was selected in all cases. The reason for this was that at higher flow rates the separation efficiency decreased because of a shorter interaction time between the matrix material and the nanoparticles. Lower flow rates improved the separation performance only slightly. Fig. 2A shows the resulting chromatograms of several experiments without the application of an external magnetic field. From the consistency of the triple determination it can be seen that the experiment is highly reproducible. The double peak indicates a separation into two nanoparticle fractions. The retention times of the individual peaks correspond to those of the individual peaks of the silica and synomag nanoparticles. Based on a peak analysis, a peak resolution of 0.93 was determined. The efficient fractionation of the two nanoparticle types even without the application of an external magnetic field again proves the inherent magnetic interaction of the synomag nanoparticles with the steel beads of the column matrix. In further experiments, the fractionation could be reproducibly achieved over months with the same column.

To quantify the efficiency of the fractionation, individual samples of the effluent were collected as fractions for further analysis including elemental analysis using ICP-OES. The results of this analysis are shown in Fig. 2B. The large discrepancy in the concentrations of silica and iron can be explained by the large difference in the nanoparticle concentrations used. This difference was chosen because otherwise a photometric analysis would not have been possible. Even at low concentrations the synomag nanoparticles showed very high extinctions, which covered the extinctions caused by the silica nanoparticles. Furthermore, the weight percentage of silicon in silica nanoparticles is higher than the one of iron in synomag nanoparticles, since the latter were a composite material of maghemite and dextran. Comparing Fig. 2A and B, it can be confirmed that the first peak consists almost exclusively of silica nanoparticles. Here the iron concentration was below the detection limit. In contrast, the second peak consisted primarily of the synomag nanoparticles. Pooling samples 1–3 as purified silica nanoparticles and samples 5–10 as purified synomag nanoparticles, two hypothetical product fractions could be distinguished. Both fractions achieve a yield of more than 75%

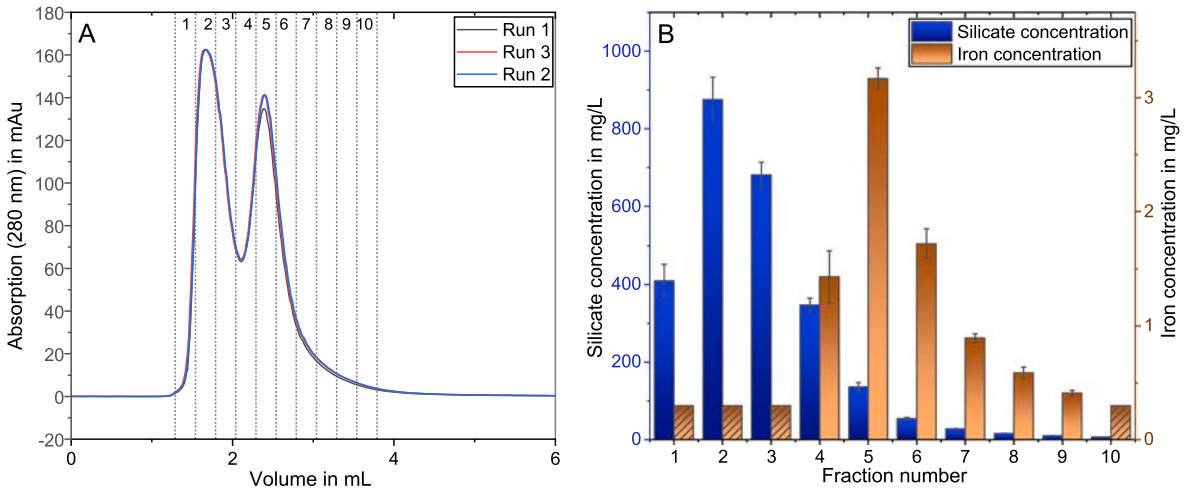

Fig. 2. Nanoparticle fractionation without the application of an external magnetic field in a chromatography column filled with a matrix of steel beads. A: Chromatogram resulting from the injection of 500 µL of a mixture of silica (1.25 g/L) and synomag (0.015 g/L) nanoparticles. In the diagram, the UV (280 nm) signal in the effluent is plotted versus the volume of the mobile phase pumped through the column. The signal shows a clear double peak with a resolution of 0.93. The experiment was conducted as triplicate. The dotted lines show the fractionation of the peak into individual samples. B: Results of the elemental analysis of the fractionated samples using ICP-OES. The elemental iron and silicon concentrations were measured. Hatched bars show results below the reliable quantification limit.

of the original amount of nanoparticles of this type in the mixture. In addition, the respective amount of the second particle type, which can be looked at as contaminant of the product, could be depleted by more than 90% if compared with the original amount in the feed, in both cases.

3.2. Nanoparticle fractionation applying an external magnetic field

In a further series of experiments, the effect of an external magnetic field was evaluated. For this purpose, the chromatography column was integrated into the center of a pair of coils with a Helmholtz arrangement. In test series, the fractionation of a mixture of silica and nanomag nanoparticles was tested applying different magnetic fields from 0 to 6.5 mT. The resulting chromatograms (Fig. 3A) show that the area of the peak representing the magnetic nanoparticles appearing in the effluent while the external magnetic field is applied (retention volume about 2–3 mL) decreases with increasing strength of the field. Similar to a previous work, an increasing shift of the peak maximum of the unbound magnetic nanoparticles can be observed. This can be attributed to a magnetic retention which increases analogous to the magnetic field [25].

The reduction of the peak area corresponds with the fraction of the magnetic nanoparticles which is temporarily separated in the column matrix until the external magnetic field is switched off. At a magnetic field of about 6.5 mT, an almost complete separation of the nanoparticles is observed. After a volume of 5 mL the magnetic field was switched off, resulting in a second, sharp nanoparticle peak in the effluent. Fig. 3B illustrates the percentage reduction of the peak area of the iron oxide peak compared to an experiment without the application of an external magnetic field. A retention of up to 83% of the original peak area was determined. The experiment with a magnetic field of 6.5 mT was also examined by ICP-OES measurements. Within the analytical accuracy a depletion of the contaminant of 100% was found for the first peak – representing the silica nanoparticles - as well as for the peak which resulted after the magnetic field was switched off (volume $>$ 5 mL) – representing the synomag nanoparticles. Since, with high magnetic fields the magnetic nanoparticles can be retarded at will, while the

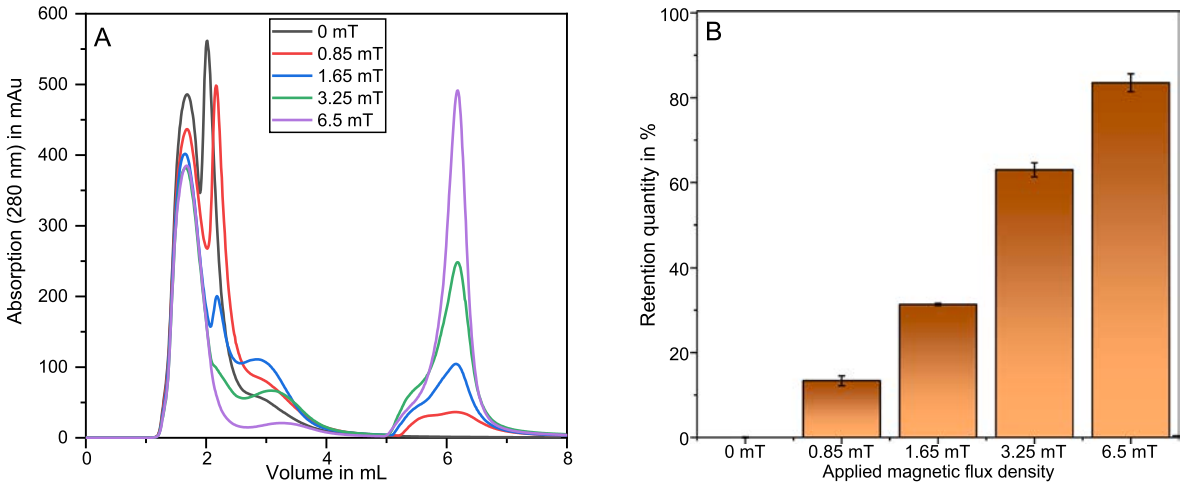

Fig. 3. Nanoparticle fractionation with the application of an external magnetic field of 0, 0.85, 1.65, 3.25, and 6.5 mT in a chromatography column filled with a matrix of steel beads. A: Chromatogram resulting from the injection of 500 µL of a mixture of silica (1.25 g/L) and nanomag (0.25 g/L) nanoparticles. In the diagram, the UV (280 nm) signal in the effluent is plotted versus the volume of the mobile phase pumped through the column. After a volume of 5 mL, the magnetic field was switched off. All experiments were conducted as triplicate. B: Photometrically determined percentage of the reduction of the peak area of the iron oxide nanoparticles compared to an execution without a magnetic field.

diamagnetic silica particles show very little effect, a baseline separation can be achieved.

3.3. Simulated moving bed experiments

The magnetic chromatography used so far is a batch process. In order to achieve a continuous nanoparticle fractionation with this novel method, the process had to be converted to a simulated moving bed chromatography. Here a movement of the chromatography matrix is simulated by a cyclic change of the interconnection of multiple identical columns. Thus, with a correctly selected switching time, a cyclic-steady state can be achieved, in which an isocratic fractionation of a feed stream into a raffinate and an extract stream is performed. For this purpose, a set-up of four columns was assembled, whereby each zone of the SMB always consisted of one column. The control of the magnetic fields was controlled by equipping each coil with its own power supply. The laboratory setup can be seen in the SI in Fig. S1.

As a first experimental series the results obtained by the SMB arrangement without the use of external magnetic fields is shown. To increase the productivity of the system, the concentration of synomag nanoparticles in this experimental series was increased to 50 mg/L. Using the experiments from the single column experiments, the Henry coefficients H_{Silica} 0.11 and $H_{synomag}$ 0.37 could be determined. The flow rates and switching times were adjusted after several iteration experiments in order to optimize the fractionation.

In Table 1., the flow rates of the separation zones of the SMBs are shown analogous to Fig. 1.

Fig. 4 shows a m_2-m_3 diagram using the triangle method, including the conditions of equation (6), as well as the operating points from previous experiments in blue and the selected operating point of the SMB process in red. The corresponding preliminary experiments can be found in the SI. By using the switching valve mentioned in chapter 2.2 the flow leaving the fourth zone could be investigated in these experiments. It was found that if the switching time of the SMB cycle is too high, silicate particles already elute from this zone, which could be seen in Fig. S3 C in the SI. This would result in an unwanted transfer of the silicate particles into the extract due to flow-through. As a conclusion of these experiments it could be determined that the flow rate ratio has to be m_4 0.325 at most to prevent this effect. In zone 3 the flow rate ratio has to be higher than at least m_3 0.33 to prevent silicate nanoparticles in the extract with this setup. For this reason, a m_3 value of 0.37 was chosen in this experiment to maintain the conditions of equation (6), but to obtain an extract as pure as possible. In Fig. 4 one can see from the triangle method that the operating point is at the edge of these conditions. This shows that without the application of an external magnetic field the operation window of the SMB magnetic chromatography is rather small.

Based on the UV progression of this SMB-process, which can be seen in Fig. 5A, it can be observed that after about 14 min, which corresponds

Table 1
Dimensionless flow rates (m_1 to m_4) for the SMB process for the separation of silica and synomag particles in a steel matrix without external magnetic field. The adjusted switching time corresponds to twice the real switching time, because the used system can integrate up to 8 separation columns.

Method-parameter and unit	No external Field
Cycle Time in min	2.80
Adjusted switching time in min	0.70
m_1	0.616
m_2	0.271
m_3	0.37
m_4	0.27
Flow extract in mL/min	1.355
Flow raffinate in mL/min	0.916
Flow feed in mL/min	0.496
Flow eluent in mL/min	1.775

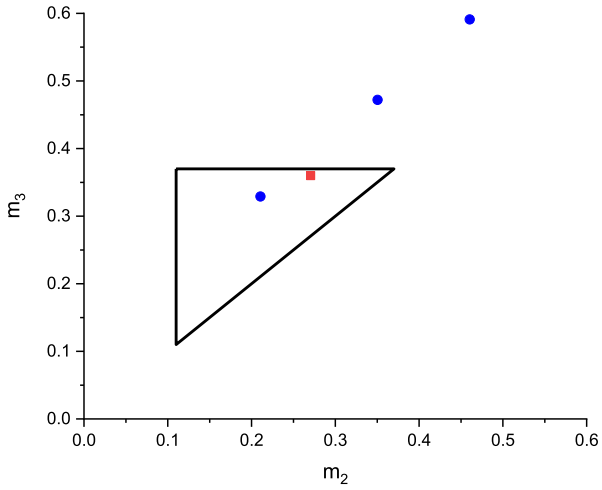

Fig. 4. m_2-m_3 diagram for the design of an SMB process for the separation of silica and synomag particles in a steel matrix without external magnetic field. The red square represents the operating point selected in the experimental series. The blue dots represent preliminary trial experiments which could be seen in the SI. (For interpretation of the references to color in this figure legend, the reader is referred to the web version of this article.)

to about five complete SMB cycles, a cyclic-steady state for the extract is reached while the raffinate shows a slightly increasing tendency of the UV-signal. This remained constant over the course of the experiments conducted. At this cyclic-steady state there is a constant fractionation process with periodic fluctuations of the nanoparticle concentrations in the extract and raffinate streams. By pooling the effluent streams over a time interval of five cycles, a feed stream can be fractionated into two product streams with consistent quality. These samples were analyzed for their elemental composition using ICP-OES (See Fig. 5B). During the first two samples, corresponding to cycles 1–5 and 6–10, gradually increasing silicon and iron concentrations were detected. This corresponds to the respective chromatograms, as the cyclic-steady state has not been reached. It can be observed that the raffinate contains pure the silica particles without contamination by synomag particles. This is consistent with the observation of the chromatogram from the single column experiments (see Fig. 2), which showed that the silicate particles have a shorter retention time and are therefore expected to end up in the raffinate. In total, 91.4% of the silica and 92.9% of the maghemite nanoparticles could be recovered in the product streams. Only 32% (w/w) of the silicate nanoparticles used were found in the raffinate, however, these showed a high purity of practically 100% (w/w). The high difference in the intensity of UV absorption between the raffinate and the extract can be explained by the presence of the synomag nanoparticles in the extract. The extract still has a high fraction of silica nanoparticles, nevertheless the purity of the synomag particles increased from 3.8% in the feed to 5.1% (w/w) in the extract. This results in a purification factor of 1.34 for the magnetic nanoparticles. This shows an incomplete fractionation. As was shown in the single column experiments, no baseline separation of the particle types was achieved without the application of an external magnetic field. Therefore, only a decrease of the silicate particles in the extract and a contaminant-free raffinate with low yield could be achieved at this point. A change in the switching time of the experiment, resulting in different dimensionless flow rates, is a critical factor here. The m_2-m_3 diagram (Fig. 4) shows that it is difficult to optimize the flow rate ratio without contaminating the raffinate stream. An overview of the results with different switching times is given in the SI in Fig. S3. Too high switching times lead to a contamination of the raffinate with magnetic nanoparticles which should be fractionated into the extract. Therefore, an improvement of the fractionation performance is required for an efficient operation of the magnetic chromatography SMB. One possibility could be to increase the effective

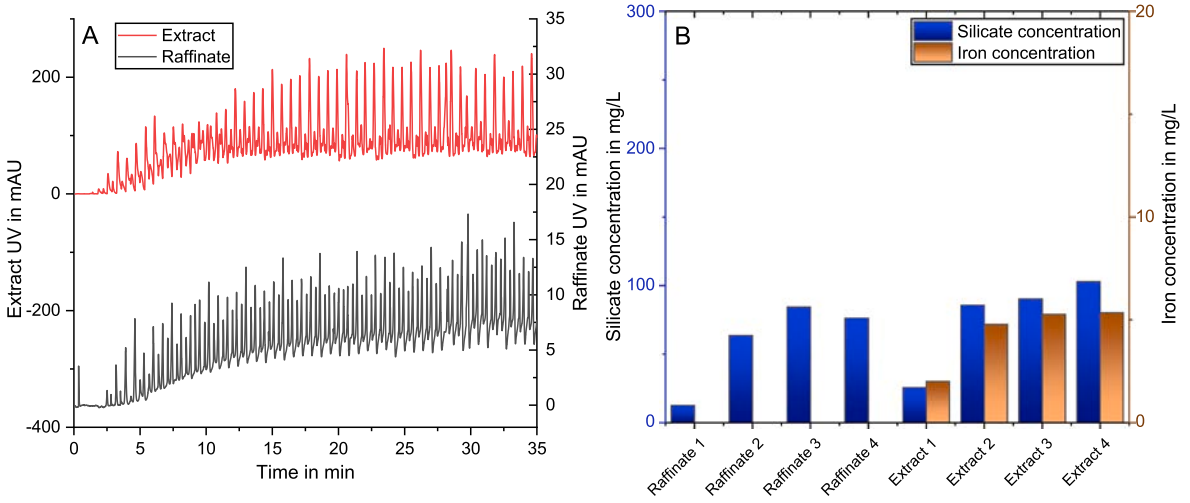

Fig. 5. Continuous nanoparticle fractionation without the application of an external magnetic field in a simulated moving bed chromatography (SMB) with four columns with matrices of steel beads. A: SMB-Chromatogram resulting from the continuous injection of 0.496 mL/min of a mixture of silica (1.25 g/L) and synomag (0.05 g/L) nanoparticles. In the diagram, the UV (280 nm) signal in the two effluents, the raffinate and the extract, is plotted versus the time that elapsed. The signal shows a periodic-cyclic progression, which is characteristic for SMB processes. The experiment was conducted as duplicate. Obtained samples were pooled over 5 SMB cycles. B: Results of the elemental analysis of the product streams using ICP-OES. The elemental iron and silicon concentrations were measured.

separation length of each zone by doubling the number of separation columns to eight. However, this would result in a substantial effort regarding the required columns, fitting, etc. and would also increase the pressure drop in the system up to level which might be critical.

As shown in the single column experiments, another approach to increase the fraction efficiency is the application of external magnetic fields, individually controlled for each column. With this operation method, a baseline separation in single column experiments could be achieved. By the help of individual Helmholtz coils in which the chromatography columns were mounted a magnetic flux density of 6.5 mT was generated in the columns located in zone 2, 3, and 4 (see Fig. 1). In expectation of an improved fractionation performance, the concentration of maghemite nanoparticles was further increased to 125 mg/L. On the basis of the controllable interaction strength by the help of an external magnetic field an improved separation efficiency of the extract should be achieved. Because of the possibility to switch off the external magnetic field, the magnetic nanoparticles in zone 1 are transported with the fluid flow and partly reach zone 2. However, within zone 2 these particles are strongly retarded by the active magnetic field and prevented from being transported into zone 3. Due to this principle the Henry coefficient of the synomag nanoparticle is freely selectable. This also made it possible to perform an operating point of the SMB with a higher dimensionless flow rate ratio m_3 to eliminate the previously observed contaminations in the extract stream. The representation of this m_2-m_3 ratio is shown in Fig. 6 with the selected operating point, which results from the process parameters in Table 2..

From this diagram it can be observed that the choice of the operating point can be greatly simplified by using the magnetic field. From the experience gained with the SMB experiments without magnetic field, a higher dimensionless flow rate ratio m_3 is advantageous reduce the silicate contamination in the extract stream. With this operation mode, further SMB experiments were carried out. The results of these experiments can be seen in Fig. 7.

The UV signal of the extract shows sharp UV peaks with the signal returning to almost 0 mAU in between the switching events (Fig. 7A). This shows that within the cycles complete elution and regeneration of the column in zone 1 has been achieved. In the case of the raffinate it can be observed that the signal shows some relatively small fluctuations and never returns to zero. This can be explained by the missing interaction between he silica nanoparticles and the column matrix. In consequence, the silica nanoparticles pass the columns at approximately the same

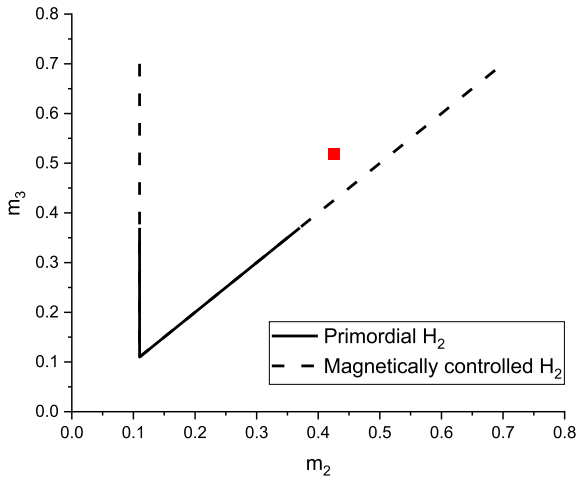

Fig. 6. m_2-m_3 diagram for the design of an SMB process for the separation of silica and synomag particles in a steel matrix with a magnetic field controlled elution. The red dot represents the operating point selected in the experimental series. (For interpretation of the references to color in this figure legend, the reader is referred to the web version of this article.)

Table 2
Dimensionless flow rates (m_1 to m_4) for the SMB process for the separation of silica and synomag particles in a steel matrix with a magnetic field controlled elution. The adjusted switching time corresponds to twice the real switching time, because the used system can integrate up to 8 separation columns.

Method-parameter and unit	Flux density: 6.5 mT
Cycle Time in min	3.04
Adjusted switching time in min	0.76
m_1	0.715
m_2	0.421
m_3	0.514
m_4	0.27
Flow extract in mL/min	1.035
Flow raffinate in mL/min	0.654
Flow feed in mL/min	0.327
Flow eluent in mL/min	1.359

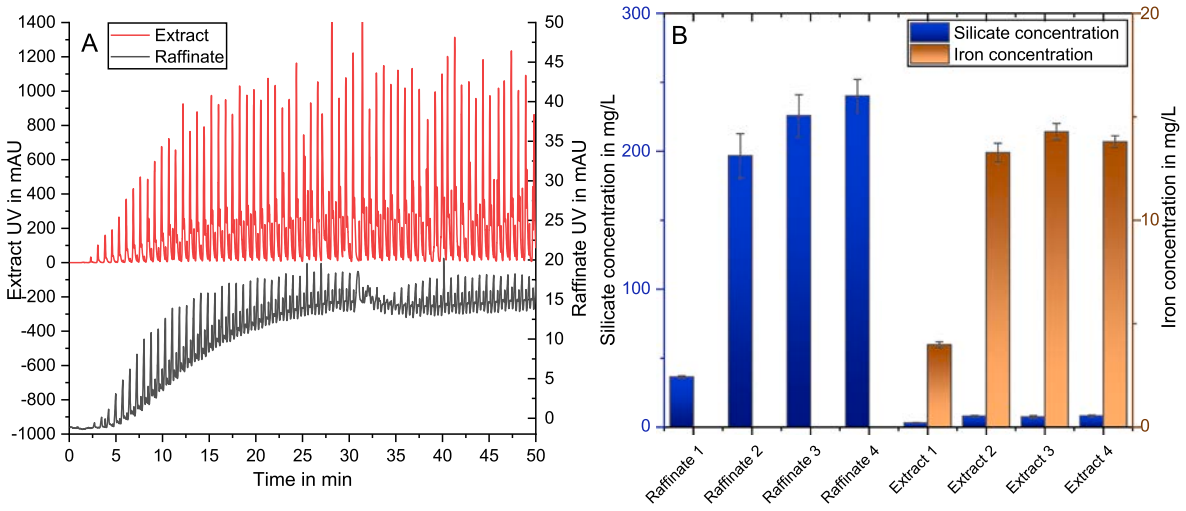

Fig. 7. Continuous nanoparticle fractionation with an application of an external magnetic field of 6.5 mT in a simulated moving bed chromatography (SMB) with four columns with matrices of steel beads. A: SMB-Chromatogram resulting from the continuous injection of 0.327 mL/min of a mixture of silica (1.25 g/L) and synomag (0.125 g/L) nanoparticles. In the diagram, the UV (280 nm) signal in the two effluents, the raffinate and the extract, is plotted versus the time that elapsed. The signal shows a periodic-cyclic progression, which is characteristic for SMB processes. The experiment was conducted as duplicate. Obtained samples were pooled over 5 SMB cycles. B: Results of the elemental analysis of the product streams using ICP-OES. The elemental iron and silicon concentrations were measured.

speed as the liquid and appear in the effluent at a constant concentration. If the elemental analyses by means of ICP-OES is considered (Fig. 7B), again a contaminant-free raffinate is visible. In contrast to the SMB experiments without the application of a magnetic field, also the extract shows a good depletion of silica nanoparticles. Consequently, the efficiency of the process could be drastically increased through the use of magnetic field controlled fractionation and the thereby possible extension of the switching time. In total, a depletion of 100% of the magnetite particles in the extract and 92% of the silicate nanoparticles in the raffinate was achieved. A purification factor of 6.96 was achieved for the synomag particles in this experiment. This observation also agrees with the assumptions from the m_2-m_3 diagram (Fig. 6). The setup allowed a continuous fractionation of nanoparticles of 50 nm diameter with a space time yield of 27.5 mg/(L*min). Furthermore, the development of a SMB setup in which the interaction between the target particles and the column matrix can be individually controlled in each zone opens up a multitude of new possibilities for novel fractionation processes. However, the presented setup will allow such gradients of the interaction strength between different columns or, if applying tailored electrical coils, even within a column. This would allow novel gradient modes of operation, for example with multimodal nanoparticle mixtures with multiple susceptibility differences, to be segregated into a single SMB process.

4. Summary and conclusions

In this study, we presented magnetic chromatography as a new method for the fractionation of equally sized nanoparticles based on their magnetic susceptibility. For the experiments, silica as well as core–shell and cluster-like iron-oxide-dextran nanoparticles were selected as three particle types of similar size and comparable density. The core of the setup developed for magnetic chromatography consisted of one or multiple columns filled with a magnetizable stainless steel matrix and surrounded by a Helmholtz coil arrangement which could superimpose an external magnetic field. In preliminary tests it showed that single-domain magnetic nanoparticles are prone to an attractive interaction with the column matrix even without the application of the external magnetic field. Therefore, a moderate fractionation (peak resolution 0.93) between these nanoparticles and diamagnetic nanoparticles also present in the injected suspension could be achieved. By using an external magnetic field, however, the fractionation efficiency could be increased up to a base line separation with peak resolutions >1.5. These fractionations had a high reproducibility and the chromatography columns showed no degradation over many experiments. Still, batch chromatography applying cyclic fractionation of small volumes of injected pulses of the suspension, is hard to scale to larger throughputs and shows low space–time yields. Therefore, both approaches (magnetic chromatography without and with the application of an external magnetic field) were transferred into a continuous process using a new variant of Simulated Moving Bed (SMB) chromatography. SMB processes allow a simple upscaling and thus throughputs of up to multiple L/h or even m^3/h. In a first test series without external magnetic fields, it could be shown that a raffinate stream including only silica nanoparticles could be obtained, however the majority of both particle types ends up in the extract stream. By applying external magnetic fields varying with the SMB zone in which the respective column operates, the process parameters could be optimized further resulting in an effective and continuous nanoparticle fractionation. The contaminant-depletions of the raffinate and extract stream reached 92 and 100%, respectively. Compared to classical processes for nanoparticle fractionation, such as high-performance centrifuges, the energy consumption of the used coils is still low. A special feature of the new fractionation process is the individual adaptability of the strength of the interaction with the matrix in each zone of the SMB. This feature opens up a multitude of new possibilities for novel operation modes, which cannot be realized with a conventional SMB. An example for such a new operation mode would be the simplified fractionation of a feed suspension into more than two product streams in a multicolumn setup.

CRediT authorship contribution statement

Carsten-Rene Arlt: Conceptualization, Methodology, Visualization, Writing - original draft, Formal analysis, Supervision. **Dominik Brekel:** Investigation, Formal analysis. **Matthias Franzreb:** Conceptualization, Methodology, Writing - review & editing, Project administration, Supervision.

Declaration of Competing Interest

The authors declare that they have no known competing financial interests or personal relationships that could have appeared to influence the work reported in this paper.

Acknowledgements

The authors acknowledge financial support by the Deutsche Forschungsgemeinschaft (DFG) within the priority program SPP 2045 (Project C11, Grant-Nr. FR 2131/6-1). Furthermore, we thank the company micromod for the contribution of experimental material.

References

[1] C.M. Welch, R.G. Compton, The use of nanoparticles in electroanalysis: a review, Anal. Bioanal. Chem. 384 (2006) 601–619, https://doi.org/10.1007/s00216-005-0230-3.
[2] A. Tschope, M. Wyrwoll, M. Schneider, K. Mandel, M. Franzreb, A magnetically induced fluidized-bed reactor for intensification of electrochemical reactions, Chem. Eng. J. 385 (2020), 123845, https://doi.org/10.1016/j.cej.2019.123845.
[3] A. Tschope, S. Heikenwalder, M. Schneider, K. Mandel, M. Franzreb, Electrical conductivity of magnetically stabilized fluidized-bed electrodes – Chronoamperometric and impedance studies, Chem. Eng. J. 396 (2020), 125326, https://doi.org/10.1016/j.cej.2020.125326.
[4] K.T. Nguyen, Targeted nanoparticles for cancer therapy: promises and challenges, J. Nanomedic. Nanotechnol. 02 (2011), https://doi.org/10.4172/2157-7439.1000103e.
[5] J.W.M. Chon, C. Bullen, P. Zijlstra, M. Gu, Spectral encoding on gold nanorods doped in a silica sol-gel matrix and its application to high-density optical data storage, Adv. Funct. Mater. 17 (2007) 875–880, https://doi.org/10.1002/adfm.200600565.
[6] L. Zhao, A. Seth, N. Wibowo, C.-X. Zhao, N. Mitter, C. Yu, A.P.J. Middelberg, Nanoparticle vaccines, Vaccine 32 (2014) 327–337, https://doi.org/10.1016/j.vaccine.2013.11.069.
[7] S.X. Wang, G. Li, Advances in giant magnetoresistance biosensors with magnetic nanoparticle tags: review and outlook, IEEE Trans. Magn. 44 (2008) 1687–1702, https://doi.org/10.1109/TMAG.2008.920962.
[8] A. Nasir, A. Kausar, A. Younus, A review on preparation, properties and applications of polymeric nanoparticle-based materials, Polym.-Plast. Technol. Eng. 54 (2015) 325–341, https://doi.org/10.1080/03602559.2014.958780.
[9] A.E. Deatsch, B.A. Evans, Heating efficiency in magnetic nanoparticle hyperthermia, J. Magn. Magn. Mater. 354 (2014) 163–172, https://doi.org/10.1016/j.jmmm.2013.11.006.
[10] A.J. Giustini, A.A. Petryk, S.M. Cassim, J.A. Tate, I. Baker, P.J. Hoopes, Magnetic nanoparticle hyperthermia in cancer treatment, Nano Life 1 (2010), https://doi.org/10.1142/S1793984410000067.
[11] S. Kayal, R.V. Ramanujan, Anti-cancer drug loaded iron-gold core-shell nanoparticles (Fe@Au) for magnetic drug targeting, J. Nanosci. Nanotechnol. 10 (2010) 5527–5539, https://doi.org/10.1166/jnn.2010.2461.
[12] Y. Chen, J.J. Wu, L. Huang, Nanoparticles targeted with NGR motif deliver c-myc siRNA and doxorubicin for anticancer therapy, Mol. Ther. 18 (2010) 828–834, https://doi.org/10.1038/mt.2009.291.
[13] V.J. Mohanraj, Y. Chen, Nanoparticles - a review, Trop. J. Pharm. Res. 5 (2007), https://doi.org/10.4314/tjpr.v5i1.14634.
[14] E.M. Hotze, T. Phenrat, G.V. Lowry, Nanoparticle aggregation: challenges to understanding transport and reactivity in the environment, J. Environ. Qual. 39 (2010) 1909–1924, https://doi.org/10.2134/jeq2009.0462.
[15] L.E. Spelter, H. Nirschl, Classification of fine particles in high-speed centrifuges, Chem. Eng. Technol. 33 (2010) 1276–1282, https://doi.org/10.1002/ceat.201000089.
[16] A. Rolland, Clinical pharmacokinetics of doxorubicin in hepatoma patients after a single intravenous injection of free or nanoparticle-bound anthracycline, Int. J. Pharm. 54 (1989) 113–121, https://doi.org/10.1016/0378-5173(89)90330-X.
[17] N. Alele, R. Streubel, L. Gamrad, S. Barcikowski, M. Ulbricht, Ultrafiltration membrane-based purification of bioconjugated gold nanoparticle dispersions, Sep. Purif. Technol. 157 (2016) 120–130, https://doi.org/10.1016/j.seppur.2015.11.033.
[18] I. Limayem, C. Charcosset, H. Fessi, Purification of nanoparticle suspensions by a concentration/diafiltration process, Sep. Purif. Technol. 38 (2004) 1–9, https://doi.org/10.1016/j.seppur.2003.10.002.
[19] M. Konrath, A.-K. Brenner, E. Dillner, H. Nirschl, Centrifugal classification of ultrafine particles: influence of suspension properties and operating parameters on classification sharpness, Sep. Purif. Technol. 156 (2015) 61–70, https://doi.org/10.1016/j.seppur.2015.06.015.
[20] M. Wu, Z. Mao, K. Chen, H. Bachman, Y. Chen, J. Rufo, L. Ren, P. Li, L. Wang, T. J. Huang, Acoustic separation of nanoparticles in continuous flow, Adv. Funct. Mater. 27 (2017), https://doi.org/10.1002/adfm.201606039.
[21] M. Hanauer, S. Pierrat, I. Zins, A. Lotz, C. Sonnichsen, Separation of nanoparticles by gel electrophoresis according to size and shape, Nano Lett. 7 (2007) 2881–2885, https://doi.org/10.1021/nl071615y.
[22] E. Lhuillier, P. Hease, S. Ithurria, B. Dubertret, Selective electrophoretic deposition of CdSe nanoplatelets, Chem. Mater. 26 (2014) 4514–4520, https://doi.org/10.1021/cm501713s.
[23] S. Süß, C. Metzger, C. Damm, D. Segets, W. Peukert, Quantitative evaluation of nanoparticle classification by size-exclusion chromatography, Powder Technol. 339 (2018) 264–272, https://doi.org/10.1016/j.powtec.2018.08.008.
[24] Nakashima Nomizu, Tanaka Sato, Kawaguchi, Magnetic chromatography of magnetic fine particles suspended in a liquid with a steel-bead column under a periodically intermittent magnetic field, Anal. Sci. 12 (1996) 829–834, https://doi.org/10.2116/analsci.12.829.
[25] C.-R. Arlt, A. Tschope, M. Franzreb, Size fractionation of magnetic nanoparticles by magnetic chromatography, J. Magn. Magn. Mater. 497 (2020), 165967, https://doi.org/10.1016/j.jmmm.2019.165967.
[26] S.N. Podoynitsyn, O.N. Sorokina, A.L. Kovarski, I.I. Levin, S.B. Simakin, High-gradient magnetic separation of nanoparticles with ferromagnetic track-etched membrane, IEEE Trans. Magn. 54 (2018) 1–8, https://doi.org/10.1109/TMAG.2018.2797918.
[27] G.D. Moeser, K.A. Roach, W.H. Green, T. Alan Hatton, P.E. Laibinis, High-gradient magnetic separation of coated magnetic nanoparticles, AIChE J. 50 (2004) 2835–2848, https://doi.org/10.1002/aic.10270.
[28] P. Fraga García, M. Brammen, M. Wolf, S. Reinlein, M. Freiherr von Roman, S. Berensmeier, High-gradient magnetic separation for technical scale protein recovery using low cost magnetic nanoparticles, Sep. Purif. Technol. 150 (2015) 29–36, https://doi.org/10.1016/j.seppur.2015.06.024.
[29] K.Y.T. Nomizu, M. Watanabe, Magnetic chromatography for magnetic fine particles using a periodically intermittent magnetic field, in: Analytical Sciences/Supplements, il77 - il80.
[30] A. Seidel-Morgenstern, L.C. Keßler, M. Kaspereit, New developments in simulated moving bed chromatography, Chem. Eng. Technol. 31 (2008) 826–837, https://doi.org/10.1002/ceat.200800081.
[31] M. Schulte, J. Strube, Preparative enantioseparation by simulated moving bed chromatography, J. Chromatogr. A 906 (2001) 399–416, https://doi.org/10.1016/S0021-9673(00)00956-0.
[32] M.D. LeVan (Ed.), Fundamentals of Adsorption: Proceedings of the Fifth International Conference on Fundamentals of Adsorption, Springer, Boston, MA, 1996.
[33] T. Krober, M.W. Wolff, B. Hundt, A. Seidel-Morgenstern, U. Reichl, Continuous purification of influenza virus using simulated moving bed chromatography, J. Chromatogr. A 1307 (2013) 99–110, https://doi.org/10.1016/j.chroma.2013.07.081.
[34] P. Satzer, M. Wellhoefer, A. Jungbauer, Continuous separation of protein loaded nanoparticles by simulated moving bed chromatography, J. Chromatogr. A 1349 (2014) 44–49, https://doi.org/10.1016/j.chroma.2014.04.093.
[35] N.B. Kondrashova, V.A. Valtsifer, V.N. Strelnikov,V.Ya. Mitrofanov, S.A. Uporov, Magnetic Properties of Silica with Mesopores Structured as MCM-48.
[36] M. Mazzotti, G. Storti, M. Morbidelli, Supercritical fluid simulated moving bed chromatography, J. Chromatogr. A 786 (1997) 309–320, https://doi.org/10.1016/S0021-9673(97)00594-3.
[37] A. Rajendran, G. Paredes, M. Mazzotti, Simulated moving bed chromatography for the separation of enantiomers, J. Chromatogr. A 1216 (2009) 709–738, https://doi.org/10.1016/j.chroma.2008.10.075.
[38] A. Rodrigues, Simulated Moving Bed Technology: Principles, Design and Process Applications, Butterworth-Heinemann, 2015.
[39] P. Biehl, M. von der Lühe, S. Dutz, F.H. Schacher, Synthesis, characterization, and applications of magnetic nanoparticles featuring polyzwitterionic coatings, Polymers (Basel) 10 (2018), https://doi.org/10.3390/polym10010091.
[40] S. Dutz, M.E. Hayden, A. Schaap, B. Stoeber, U.O. Hafeli, A microfluidic spiral for size-dependent fractionation of magnetic microspheres, J. Magn. Magn. Mater. 324 (2012) 3791–3798, https://doi.org/10.1016/j.jmmm.2012.06.014.